

Self-accelerating Dirac particles and prolonging the lifetime of relativistic fermions

Ido Kaminer^{1,2*}, Jonathan Nemirovsky¹, Mikael Rechtsman¹, Rivka Bekenstein¹ and Mordechai Segev¹

The Aharonov-Bohm effect predicts that two parts of the electron wavefunction can accumulate a phase difference even when they are confined to a region in space with zero electromagnetic field. Here we show that engineering the wavefunction of electrons, as accelerating shape-invariant solutions of the potential-free Dirac equation, fundamentally acts as a force and the electrons accumulate an Aharonov-Bohm-type phase—which is equivalent to a change in the proper time and is related to the twin-paradox gedanken experiment. This implies that fundamental relativistic effects such as length contraction and time dilation can be engineered by properly tailoring the initial conditions. As an example, we suggest the possibility of extending the lifetime of decaying particles, such as an unstable hydrogen isotope, or altering other decay processes. We find these shape-preserving Dirac wavefunctions to be part of a family of accelerating quantum particles, which includes massive/massless fermions/bosons of any spin.

In 1958, Aharonov and Bohm (AB) predicted that two parts of the wavefunction of an electron can accumulate a phase difference even when they are confined to a region in space with zero electromagnetic (EM) field¹. The AB effect proved that the EM vector potential is a physical entity (up to a gauge change), affecting the outcome of experiments directly, not only through the fields derived from it. The effect was later generalized by Berry to general topological effects² and observed in many experiments. Recently, an AB effect was observed for photons, which cannot interact with an EM potential, but instead are affected by an effective magnetic field created through temporal modulation of the refractive index^{3–5}. Analogous pseudofield effects also occur in other areas, ranging from gravitation^{6,7} and solid state^{8–12} to photonics^{11–13} and cold atoms^{14–17}, where engineered topology can create effective EM potentials. Such effective potentials can often be probed directly, even including their gauge, as they are artificial. It is now clear that a real EM potential is no longer required for an AB-type effect. But, can such effect exist even without structure, in free space?

Paul Dirac's inspiring quotation, 'God used beautiful mathematics in creating the world', is manifested time and again in science, not least in the equation Dirac himself derived to describe the wave motion of relativistic particles¹⁸. Dirac's equation introduced the fermionic spinor and predicted antimatter, and its generalizations described the dynamics of a large variety of quantum particles. For decades, however, Dirac fermions and their associated phenomena (for example, Klein tunnelling) remained in the realm of high-energy physics and were not observed in experiments. In recent years, research on graphene has introduced a new kind of system described by the Dirac model¹⁹. The same model is also found in novel artificial materials such as honeycomb photonic lattices²⁰, bosonic condensates modulated by optical lattices^{21,22}, and other forms of 'artificial graphene'^{21,23,24}, having a Dirac cone band structure corresponding to massless Dirac particles. Further Dirac-like dynamics associated with massive Dirac particles is now found in hyperbolic metamaterials^{25,26}. The common principle underlying Dirac-like systems is their unusual band structure, which exhibits two bands intersecting at a single point. In the vicinity of the

intersection point, the band structure is conical (or hyperbolic), therefore wavepackets residing near this point obey the massless (or massive) Dirac equation. As a consequence of these modern realizations of the Dirac model, a variety of intriguing physical phenomena have been observed and proposed: Klein tunnelling^{21,27}, negative magnetoresistance²⁸, conical diffraction²⁰, the quantum Hall effect at room-temperature and Berry phase effects in graphene⁸. In recent years, further effects arising from the Berry phase were found in a variety of settings, including various Dirac models, honeycomb lattices, plasmonic structures, harmonically modulating photonic systems, and more^{3–7,29}. In all of these, the geometrical properties of the Hamiltonian in some parameter space include a singularity, which contributes a non-trivial phase factor when encircled. Specifically, for optical beams in three-dimensional (3D) free space, Berry's phase in 3D can attain any value between 0 and 2π (ref. 30). However, even in that simple scenario, the mirrors used in the optical system create the non-trivial geometry responsible for the non-zero Berry phase.

Here, we predict self-accelerating Dirac wavepackets exhibiting accumulation of Berry phase as a direct outcome of their own dynamics in 2D flat free space. We show that such unusual dynamics of Dirac wavepackets mimics the dynamics of free charges under the influence of a true EM field: accelerating even though no field is acting on them, with the entire dynamics resulting from their initial conditions. We find that these geometric phase effects carry over to 3D, and also occur for many kinds of wavepackets obeying scalar wave equations such as the Helmholtz, Klein-Gordon and Schrödinger equations. In all of these, a non-trivial geometric phase can be accumulated even when the system has no physical geometry or potential whatsoever. This exciting effect is a unique property of the most intriguing family of wavefunctions: self-accelerating wavepackets.

Research on self-accelerating wavepackets has developed rapidly since its introduction into optics³¹. In optics, an ideal paraxial accelerating beam follows a parabolic trajectory while preserving its structure indefinitely as a non-diffracting wavepacket. This effect arises from interference: waves emitted from all points maintain a propagation-invariant structure that shifts laterally on a curved

¹Physics Department and Solid State Institute, Technion—Israel Institute of Technology, Haifa 32000, Israel. ²Department of Physics, Massachusetts Institute of Technology, 77 Massachusetts Avenue, Cambridge, Massachusetts 02139, USA. *e-mail: kaminer@tx.technion.ac.il

trajectory. Consequently, the wavepacket actually accelerates itself by means of interference. Note that the total momentum carried by these accelerating solutions is conserved, even though every local part of the wavefunction is accelerating. There is no contradiction, because any decaying envelope that ensures the energy is finite also restricts the acceleration to occur over a finite range in space and time. Physically, what matters are the local effects (which depend on the local wavepacket), because measurements are always carried over a finite range. This phenomenon has led to many intriguing ideas, ranging from particle guidance along curves³², curved laser-induced plasma channels³³, accelerating temporal pulses in dispersive media³⁴, and even self-trapped shape-preserving accelerating beams in nonlinear optics^{35–37}. Furthermore, the recent discovery of self-accelerating beams of the Maxwell equations³⁸ has led to the insight that accelerating wavepackets are a universal phenomenon, common to very many wave systems in nature: including general EM fields, time-harmonic acoustic, elastic and surface waves in fluids, and even EM waves in curved space³⁹. The same concept applies in quantum mechanics, where recently the wavefunction of a single electron was shaped to yield an accelerating electron wavepacket⁴⁰. Notably, ref. 40 was the first observation of any self-accelerating quantum wavepacket, in the spirit of the original prediction of Berry and Balazs⁴¹. In all of these systems, irrespective of their physical settings—the basic property of the accelerating wavepacket is common to all: the wavepacket moves as if it is under the influence of a force, or a linear ‘effective potential’ (as discussed in early works on this subject^{31,41}).

In what follows, we present shape-preserving accelerating wavepackets governed by the Dirac equation. We show that such wavepackets mimic the properties of particles moving under the influence of a real potential, not only in following exactly the same acceleration trajectories but also in exhibiting relativistic effects such as time dilation and space contraction. Most importantly, owing to the shape-preserving property, these relativistic effects correspond to an AB phase, which was thus far considered to be restricted to systems where true potentials or particular structure must be present. Thus, any measurements taken along the trajectory cannot distinguish between a true potential and this ‘effective potential’, whose action is engineered through the initial conditions of the wavepacket. The effects of this virtual force are measurable to the same extent as any physical force. This conceptual insight emphasizes the importance of this ‘effective potential’—it gives a complete model that explains all effects along the trajectory of the wavepacket, and therefore has direct implications in many quantum systems. For example, an engineered wavepacket of a muon can have longer lifetime thanks to the time dilation we find here. In a similar vein, any radioactive decay process may be altered by proper preparation of the initial quantum wavepacket. These phenomena can be observed in various settings, for example, optical waves in honeycomb photonic lattices or hyperbolic metamaterials, and matter waves in honeycomb interference structures. To understand the implications of this ‘effective potential’, we begin by deriving the self-accelerating Dirac wavepacket.

Consider a positive energy plane-wave solution $\psi_{v=0}$ of the free space Dirac equation, which describes a plane wave of velocity zero ($v=0$)

$$i\hbar\gamma^\mu\partial_\mu\psi - mc\psi = 0 \quad \psi_{v=0} = \begin{pmatrix} 0 \\ -1 \\ 0 \\ 1 \end{pmatrix} e^{i\frac{mc}{\hbar}ct} \quad (1)$$

where m is the mass of the electron, c is the speed of light, \hbar is Planck’s constant, t is time, and γ^μ are the 4×4 gamma matrices

in the Weyl basis. The concept described here holds for any spatial dimension. For simplicity, we describe the case of a single spatial dimension, where equation (1) translates to

$$\begin{pmatrix} -mc & i\hbar\left(\frac{1}{c}\partial_t + \partial_z\right) \\ i\hbar\left(\frac{1}{c}\partial_t - \partial_z\right) & -mc \end{pmatrix} \begin{pmatrix} \psi_2 \\ \psi_4 \end{pmatrix} = 0 \quad (2)$$

where $\psi = \psi(z, t)$ is a spinor describing the electron and ψ_2, ψ_4 are the two components of the spinor. In this setting of one spatial and one temporal dimension, the other pair of components (ψ_1, ψ_3) is fully degenerate with ψ_2, ψ_4 . Boosting $\psi_{v=0}$ along the z -direction yields another plane wave with a phase front evolving along $[ct \cosh(b) - z \sinh(b)]mc/\hbar$, which corresponds to velocity $v = c \tanh(b)$, or equivalently $\gamma = \cosh(b)$. These can also be conveniently described by the Rindler coordinates, or hyperbolic coordinates (see Supplementary Section VI, for further discussion on the choice of coordinates). The natural way to construct an accelerating wavepacket is to superimpose all such plane waves, with appropriate relative phase:

$$\begin{aligned} \Psi_\alpha(z, t) &= \int_{-\infty}^{\infty} e^{i\alpha b} h(b) \text{boost}_b\{\psi_{v=0}\} db \\ &= \int_{-\infty}^{\infty} \begin{pmatrix} 0 \\ -e^{-b/2} \\ 0 \\ e^{b/2} \end{pmatrix} e^{i\alpha b} h(b) e^{i\frac{mc}{\hbar} \cosh(b)ct - i\frac{mc}{\hbar} \sinh(b)z} db \quad (3) \end{aligned}$$

where α is a parameter controlling the relative phase, directly relating to the acceleration, and $h(b)$ is a decaying envelope function we introduce to ensure that the total probability is unity. Unlike the Airy beams, which are not square-integrable (hence cannot represent a probability function^{31,41}), here Ψ_α has a finite extent in space, and any decaying envelope would suffice for spin 1/2 (spin zero requires no decaying envelope at all). Figure 1a shows the 1D wavefunction accelerating along the z direction while exhibiting a shape-preserving form that increases its velocity, moving along a hyperbolic trajectory.

We now focus on the new physics revealed by these accelerating Dirac particles, while not concentrating on describing the underlying mathematics. We note, however, that there is also considerable beauty in these accelerating solutions: their structure, trajectory and exotic mathematical features, such as the singular point they all exhibit (see Supplementary Section VI for the relation of these wavepackets to the modified Bessel function of the second kind of imaginary order, which can explain many of the mathematical features). We emphasize that our solutions show for the first time that there exist accelerating shape-preserving solutions of the Dirac equation, in 1D, 2D and 3D. The methodology of generalizing to more than 1D is described in Supplementary Section I. For further details and comparison to other accelerating wavepackets see Supplementary Sections II and III.

This construction in equation (3) yields a wavepacket Ψ_α (Fig. 1a) that is ‘boost invariant’—that is, an observer moving at any velocity along the z axis sees the exact same wavepacket up to a phase $\text{boost}_b\{\Psi_\alpha\} = \exp(i\alpha b)\Psi_\alpha$. This ‘boost invariance’ is what causes the wavepacket to behave as a self-accelerating particle: it explains the self-acceleration and the tendency of the wavepacket to preserve its shape. Without this shape-preserving feature (that is, if the wavefunction varies during evolution) it would be difficult to associate the physical behaviour of the wavepacket with acceleration³¹ and—most importantly—with acceleration of a physical particle (for discussion on non-shape-preserving accelerating wavepackets see Supplementary Section II).

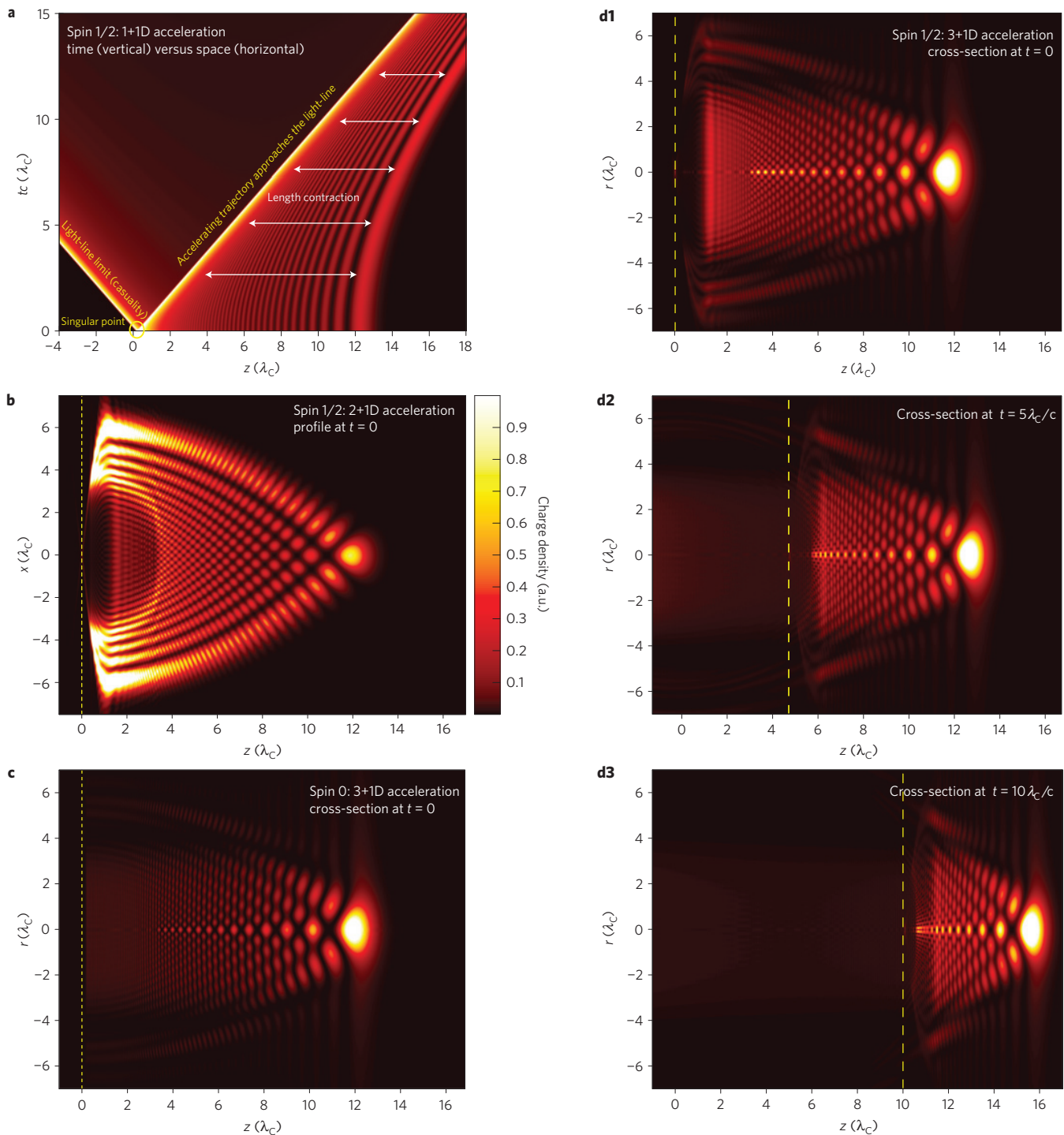


Figure 1 | Accelerating Dirac particles. Expectation value of the charge density $\rho(z, t) = |\Psi^1_\alpha|^2 + |\Psi^2_\alpha|^2 + |\Psi^3_\alpha|^2 + |\Psi^4_\alpha|^2$ of a self-accelerating Dirac wavepacket Ψ_α , exhibiting space contraction and shape-preserving dynamics. An observer moving at any velocity along the z axis sees the exact same wavepacket up to a phase boost. In all plots, $\alpha = 80$ and h presents truncation for $b = \pm 5$ (in **a, c**) or $b = \pm 3$ (in **b, d**). Bright colours represent higher charge densities (the colourbar is saturated for presentation clarity). The singular point is where the oscillations of the wavefunction reach an infinite rate, causing part of the density to scatter to the left, ensuring momentum conservation. **a**, The 1+1D case, given by equation (3). The singular point emits the left-propagating part of the wavefunction. This occurs owing to the finite extent of the envelope h , which limits the range for which the propagation is shape-preserving. The white arrows signify the spatial contraction due to the relativistic speeds. **b**, Accelerating wavepacket of the Dirac equation in 2+1D, at $t = 0$. a.u., arbitrary units. **c**, Accelerating wavepacket of the Klein–Gordon equation (spin 0) in 3+1D. Shown is the cross-section at $t = 0$. **d1–d3**, Snapshots of the cross-section of an accelerating wavepacket of the Dirac equation in 3+1D at three consecutive times ($(t_0, t_1, t_2) = 0, 5, 10$ in units of $\lambda_{\text{Compton}}/c$).

Figure 1b–d presents examples of accelerating Dirac wavepackets of higher dimensions. Figure 1b presents the solution for 2+1D, at $t = 0$. Figure 1c presents the solution of the Klein–Gordon

equation for 3+1D, at $t = 0$. Figure 1d shows solutions in two spatial dimensions and time (henceforth 3+1D), at three consecutive times (t_0, t_1, t_2) , exhibiting the contracted-length and shape-preserving

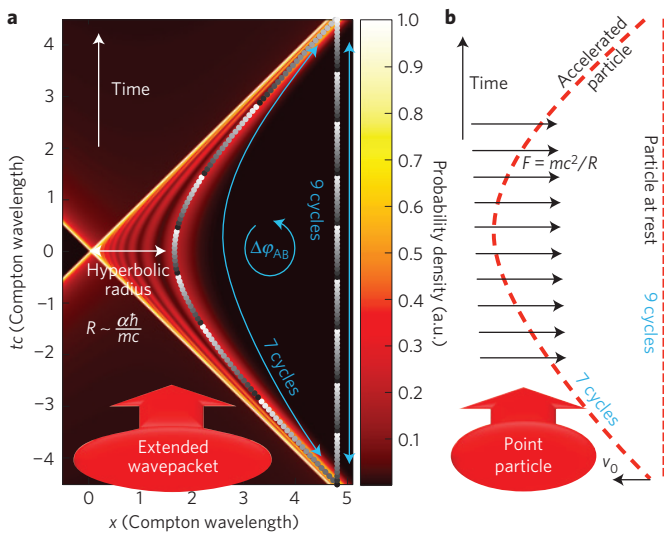


Figure 2 | The ‘twin-paradox’ gedanken experiment. **a**, The proper times of the two twins are marked on the probability density plot, showing a different amount of time that passes for each twin (seven phase cycles of 2π versus nine cycles). **b**, Trajectory of a particle under the influence of a force—emphasizing the equivalence between the accelerating Dirac wavepacket and the true particle, in terms of the trajectory, relative time dilation and AB phase. For this plot we choose $\alpha = 12$ and \hbar that presents truncation in $b = \pm 5$.

evolution, as in Fig. 1a. These examples show how rich the behaviour of accelerating Dirac wavepackets can be in 2D and 3D (see Supplementary Section I for further details). However, they all exhibit the same basic properties, such as the singular point in Fig. 1a, which is shown in the other panels (b–d) as a dashed yellow line. The singular point emits the left-propagating part of the wavefunction, which occurs owing to the finite extent of the wavepacket. This finite extent has two implications: it sets a finite limit on the range for which the wavepacket exhibits shape-preserving acceleration, and it explains how momentum is conserved while the wavepacket is accelerating. Namely, the left-propagating part balances the momentum of the rest of the wavepacket, which is accelerating to the right.

Let us now discuss the physical meaning of these exotic particles, and show they exhibit the behaviour of ordinary accelerating particles. Describing these particles as waves allows engineering the wavepacket so as to control relativistic properties, altering the proper time, and causing length contraction. To do that, we introduce hyperbolic coordinates, which are best suited to describe the dynamics in the relativistic accelerating frame: $(z, ct) = (R \cosh(\tau c/R), R \sinh(\tau c/R))$, where R is the hyperbolic radius ($c^2 t^2 = z^2 + R^2$) and $\tau c/R$ is the hyperbolic phase, which is a convenient notation as τ is exactly the proper time of a particle accelerated to relativistic speeds along this hyperbolic trajectory. By transforming the spinor wavefunctions (just ψ_1, ψ_3 in the 1+1D case) to these coordinates, one can show that R describes the hyperbolic trajectory on which each of the lobes of the accelerating wavepacket evolves. Importantly, the evolution of the wavepacket in these coordinates is shape-preserving: each lobe is strictly stationary on a specific value of R , whereas the main lobe (rightmost in all panels in Fig. 1) satisfies $R \sim (\alpha \hbar)/(mc)$, with the approximation becoming exact for $\alpha \gg 1$. Even more importantly, each of the spinor’s wavefunctions (ψ_1, ψ_3) accumulates a phase $\alpha \operatorname{asinh}(ct/R)$ which can be expressed using the proper time as $\alpha \tau c/R$. We note that τ is not just a convenient notation; rather, in the absence of any external potential, the accumulated phase is proportional to the particle’s proper time along a fixed hyperbolic trajectory, hence

τ is a measure of the clock of our accelerating wavepacket. This insight is analogous to the ‘twin-paradox’ gedanken experiment proposed by Einstein⁴². Namely, we launch a self-accelerating Dirac particle (described by $\Psi_\alpha(z, t = -t_0)$) with initial velocity to the left but acceleration to the right. At the same initial time $t = -t_0$, we position another Dirac particle at the same initial position at rest. We then let the dynamics evolve according to equation (1) or (2), and measure the difference in the clocks of such particles when they meet again at $t = t_0$ (left panel in Fig. 2). We find the difference in their clocks to be $2t_0 - 2t_\alpha \operatorname{asinh}(ct_0/R)$, where we use the notation $t_\alpha = (\alpha \hbar)/(mc^2)$, which equals α divided by the Compton frequency. Interestingly, as in the ‘twin-paradox’, there is a difference in their clock times, which means that less time has passed for the accelerating Dirac wavepacket that has gone through the longer path in spacetime. For $\alpha \gg 1$, the difference in clock times can be written as $2t_0 - 2t_\alpha \operatorname{asinh}(t_0/t_\alpha)$, which exactly matches the proper time difference of a relativistic particle that moves along the same trajectory as the accelerating wavepacket does. This interesting ‘coincidence’ is an indicator of a much deeper phenomenon: we argue that when the interference of the accelerating wavepacket creates an accelerating trajectory, it also induces a fictitious force acting on itself along that trajectory: the force that ‘would have been there’ to accelerate a true particle along this trajectory. Thus, the acceleration of the wavepacket is more than ‘just’ interference. Rather, the interference effect, arising strictly from the initial conditions on the wavepacket, induces a fictitious force acting on the wavepacket as if it were a true particle, with all of the accompanying effects it causes. In a broader perspective, just as the Aharonov–Bohm effect has proved that the EM vector potential is a true physical entity, the inevitable outcome of our findings here is that ‘self-acceleration’ acts as a force even though there is no external potential in the system whatsoever.

To show that indeed the wavepacket evolves as if a force were exerted on it, we calculate the EM potential A_μ that would normally cause the phase pattern we see along the trajectory. To achieve that, we perform the reverse calculation of the AB phase

$$\Delta\varphi = \frac{q}{\hbar c} \int_{\text{trajectory}} A_\mu dx^\mu \quad (4)$$

By using the expression of the phase along the trajectory $\alpha \tau c/R$ from above, and the shape-preserving property—which is essential for this argument—we find that only the following potential can satisfy equation (3) along the trajectory (further details in Supplementary Section IV):

$$(qA_0, qA_3) = (R \cosh(\tau c/R) - \tau c \sinh(\tau c/R), \tau c \cosh(\tau c/R) - R \sinh(\tau c/R)) \hbar c \alpha / R^2 \quad (5)$$

where q is the charge associated with the wavepacket. Notice that the effect is independent of the charge q . Finally, deriving the fields from this induced potential, we obtain a constant electric field in the lab frame: $q\mathbf{E} = -\hat{z} \hbar c \alpha / R^2$. Strikingly, substituting the relation $\alpha \sim mcR/\hbar$ (satisfied around the main lobe of the wavepacket), we find $q\mathbf{E} = -\hat{z} mc^2/R$, which is the force that accelerates a particle along the same (hyperbolic) relativistic trajectory, while experiencing the same time dilation, as our accelerating Dirac wavepacket. Furthermore, this force is exactly the ratio of the electron rest energy (mc^2) to the trajectory radius R . For a discussion about extending this result to the side lobes of the wavepacket, see Supplementary Section V. A direct conclusion from equations (4) and (5) and Fig. 2 is that the phase accumulated along the trajectory, $\alpha \operatorname{asinh}(ct/R)$, is a type of AB phase (formally, it is a type-II AB effect because the particle is subject to a non-vanishing field; still, the same (equation (4)) describes the AB phase⁴³).

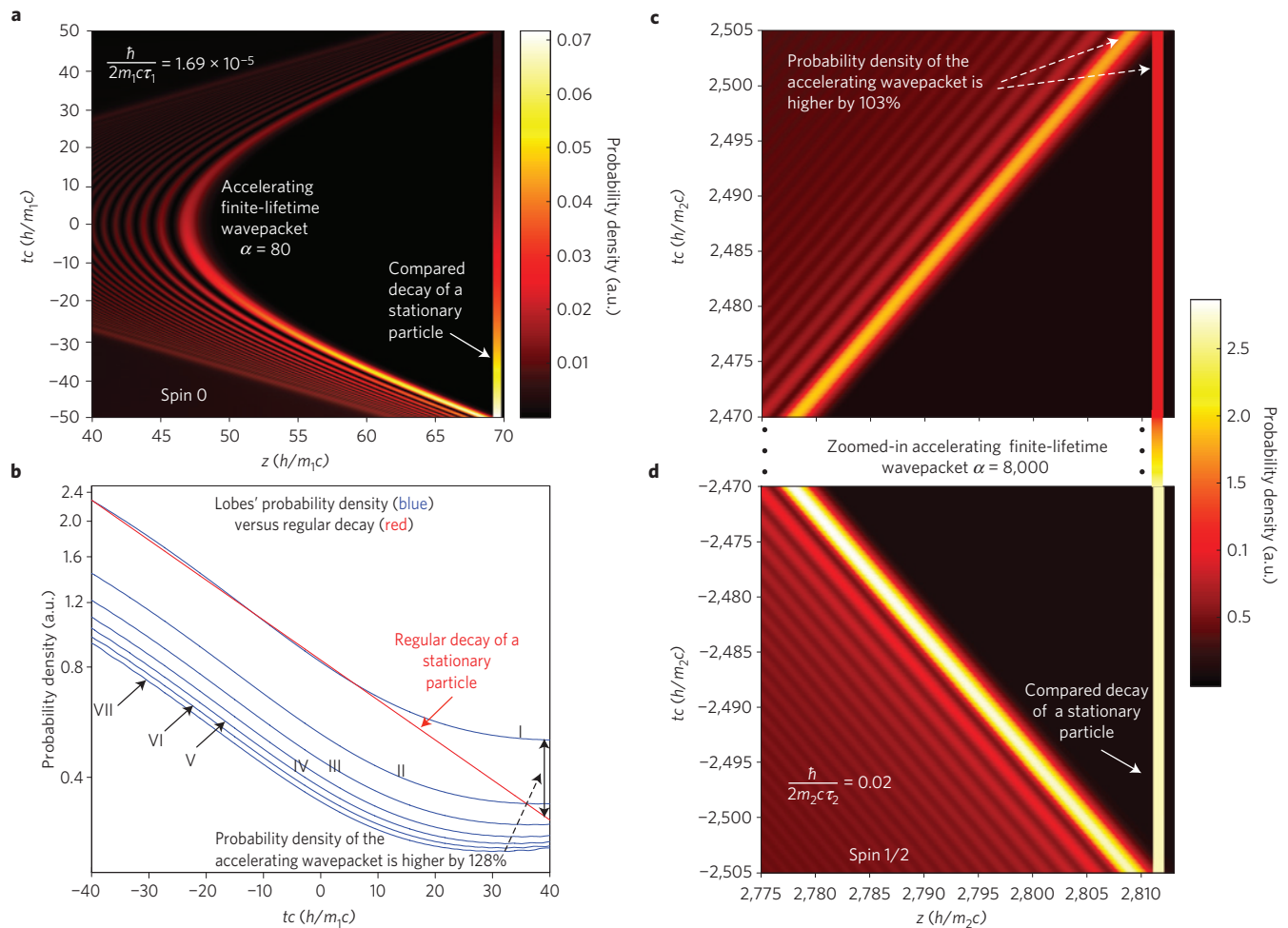


Figure 3 | Extending the lifetime of an unstable particle through self-acceleration. **a**, Probability density of a decaying self-accelerating wavepacket, compared with that of a stationary decaying particle. This example is for spin 0, $\alpha = 300$, truncation h at $b = \pm 2$. The mass m_1 and mean lifetime τ_1 represent the hydrogen isotope ^7H , which has a very short lifetime (imaginary-to-real energy ratio $\hbar/(2m_1c^2\tau_1) = 1.69 \times 10^{-5}$). **b**, The corresponding probability density decay of the first seven lobes as a function of time in the lab frame (blue curves), compared with the decay of the stationary particle (red curve). The stationary particle decays faster than the lobes of the accelerating wavepacket—its exponential decay corresponds to lifetime $\tau = 39.8\hbar/(m_1c^2)$ whereas the lifetime of the main lobe of an accelerating ^7H wavepacket is $\tau = 59.2\hbar/(m_1c^2)$, representing a 128% change in probability density over a time span of $\tau = 100\hbar/(m_1c^2)$. **c**, Two zoomed-in sections of an accelerating wavepacket of spin 1/2, $\alpha = 8,000$, and truncation h at $b = \pm 2$. The mass m_2 and mean lifetime τ_2 are of the Higgs boson, which has imaginary-to-real energy ratio of $\hbar/(2m_2c^2\tau_2) = 0.002$. The lifetime of the main lobe is longer than that of the stationary lobe by more than a factor of three ($\tau = 14,325\hbar/(m_2c^2)$, $\tau = 4,742\hbar/(m_2c^2)$ respectively), representing a 103% change in probability density over a time span of $\tau = 5,010\hbar/(m_2c^2)$.

As such, the phase difference in a scenario such as Fig. 2 is $2t_0mc^2/\hbar - 2\alpha \operatorname{asinh}(t_0/\alpha mc^2/\hbar)$. We emphasize that this AB effect is relativistic, because it results from the hyperbolic coordinates. The implication of this result is profound: an AB-like phase can be accumulated in the absence of any EM potential and without any geometry to emulate an effective potential. That is, engineering the initial conditions of the wavepacket is all that is required to generate an AB phase. This has a fascinating implication—engineering the initial conditions not only creates an effective acceleration and phase accumulation, but can also affect the properties of relativistic particles. Below we present an example showing that engineering the initial conditions to create a self-accelerating wavepacket extends the proper time of a decaying Dirac particle, thus prolonging its lifetime.

When a quantum state has a finite lifetime, it can be phenomenologically expressed by an exponentially decaying wavefunction—that is, assigning an imaginary part to the energy of this state⁴⁴. Examples include, but are not limited to radioactive decays, excited two-level systems, atoms, molecules and quantum dots, coupled to the environment or decaying through tunnelling,

gradually deteriorating condensates, coupled waveguide systems, and decaying fundamental particles such as muons and neutrons. For our case of the Dirac equation (that actually describes many of these systems), one adds the finite lifetime by replacing $mc/\hbar \rightarrow mc/\hbar + i/(2\tau_0c)$. In this modified Dirac equation the new parameter τ_0 represents the mean lifetime of the particle when it is at rest. To clarify this, consider a particle with velocity $v = \beta c$. Such a particle is described by a plane-wave solution of the modified Dirac equation (modified equation (1)):

$$i\hbar\gamma^\mu\partial_\mu\psi - \left(mc + \frac{i\hbar}{2\tau_0c}\right)\psi = 0$$

$$\psi_{v=\beta c} = \begin{pmatrix} 0 \\ -e^{-b/2} \\ 0 \\ e^{b/2} \end{pmatrix} \exp\left(\left(\frac{imc^2}{\hbar} - \frac{1}{2\tau_0}\right)\left(\gamma t - \beta\gamma\frac{z}{c}\right)\right) \quad (6)$$

where to relate to the hyperbolic coordinates we use $\gamma = \cosh(b)$ and $\beta = \sinh(b)$. When calculating the probability density, we are

left with $\exp(-\gamma t/\tau_0)$, which reveals that the lifetime is extended by a factor of γ —as expected.

To study the evolution of self-accelerating wavepackets in the modified Dirac equation, we use the same initial conditions introduced in equation (3) (which led to Figs 1a and 2). The evolution of this decaying–accelerating Dirac wavepacket is presented in Fig. 3a. It still contains the familiar features of acceleration from the above figures; however, it also shows pronounced decay. To compare this wavepacket to a stationary Dirac particle, we plot the probability of a plane-wave solution with $v=0$ as a horizontal line with gradually changing colour in Fig. 3a. Having both the self-accelerating particle and a stationary particle is the exact same configuration as the twin-paradox shown in Fig. 2—where we showed an AB-type phase difference, and a difference in the proper time. Figure 3b reveals a difference in the decay patterns between the two wavepackets, manifested in the comparison between the evolutions of the probability densities as a function of z . This clearly shows that the self-accelerating Dirac wavepacket slows down the decay of the main lobe, thus prolonging its lifetime. The slower decay is of course a local phenomenon, which we measure for each lobe individually. However, even being a local phenomenon, it does not require the other lobes to compensate for the slowed-down decay of the main lobe by exhibiting a faster decay. Instead, we find that the decay of the side lobes is also slower (Fig. 3b). There is no conservation law for the proper time or for the total decay rate, hence the entire wavepacket can indeed decay more slowly, exhibiting an extended lifetime—time dilation—without contradicting any law of nature.

For the two examples presented in Fig. 3, we chose particles with very short lifetimes. Because equation (6) can be scaled with respect to its mass, the only quantity that matters is the ratio between the imaginary and real parts of the rest energy. We chose 1.69×10^{-5} for Fig. 3a,b and 2×10^{-3} for Fig. 3c,d, corresponding to the hydrogen isotope ^7H and the Higgs boson, respectively. These particles have such a short lifetime that they cannot be considered stable particles, but are referred to as propagating resonances, which means they exist only as intermediate states in some scattering process in a particle physics experiment. We emphasize that even in such an extreme scenario, shaping these wavepackets still has a practical meaning: the measurements carried out on the final state emitted from the process will be altered in response to a change in the properties of the resonant-state particle. In reality, such an effect can be realized by engineering the wavefunction of one of the initial particles starting the scattering process. This will shape the wavefunction of the intermediate state, which will affect the properties of the emerging state.

Clearly, the effective force induced by the self-accelerating wavepacket exhibits the intriguing additional feature of altering its lifetime. This prolonged lifetime agrees with the time dilation discussed above, just as expected from ordinary particles moving at relativistic speeds. But unlike ordinary particles, the slowed-down decay happens without an external force. We showed that although the self-acceleration is the result of interference of the wavepacket's constituents, the implication affects far more than just the phase of the wavepacket. This AB-like phase effect causes changes to the decay rate, which proves that it affects relativistic properties of the particle, such as its proper time.

Before closing, it is important to discuss the possibility of testing our findings in experiments. There are a number of different platforms for achieving this. For example, photonic crystal slabs have been shown to exhibit hyperbolic dispersion akin to Dirac physics⁴⁵. Therefore, launching shaped pulses into such a spatially varying dielectric environment will allow the observation of the Aharonov–Bohm phase and the time dilation described here. Namely, the light propagating on a longer trajectory will experience a smaller time dilation, as presented in

Fig. 2. Alternative experiments include monitoring the temporal dynamics in exciton–polariton condensates²⁴ and ultracold atoms²², both in honeycomb lattices, with proper preparation of the initial wavefunction.

Interestingly, the AB phase and the time-dilation effects can also potentially be observed with actual electrons. Temporal shaping of the electronic wavefunction would require methods relying on ultrafast electron microscopy⁴⁶ plus shaping the optical excitation pulse. Here, a specifically shaped laser pulse hitting a photocathode will generate a short single-electron pulse imprinted with the structure described in equation (3). An alternative method is to directly shape the already accelerated relativistic electron beam. This can be done using a holographic mask, relying on the variation in phase delay experienced by high-velocity electrons passing through a mask patterned to have a varying thickness on the nanoscale⁴⁰. This method requires an additional step, because spatial modulation of the phase has to be translated to temporal shaping in $z-t$, giving a different phase and amplitude to different electron wave constituents of different velocity. Indeed, splitting different velocity components to different transverse translations is readily done by magnetic fields acting as prisms for electrons, and magnetic lenses. For further details and parameter estimates see Supplementary Section VII. An additional realization in a different platform would be the spatial analogue of the AB phase and the time-dilation effects. This can be directly observed in various photonic systems, exploiting the mathematical analogy between space and time: if one space coordinate takes the place of the temporal coordinate, then acceleration becomes equivalent to ‘beam bending’. Thus, a spatial AB phase can be observed in honeycomb photonic lattices²⁰, hyperbolic metamaterials²⁵, or biaxially birefringent crystals⁴⁷. In such spatial systems, the AB phase and time-dilation effects would manifest in the fact that an optical beam propagating at a longer trajectory will accumulate phase at a slower rate, counter to Fermat's principle. Altogether, we envisage a number of viable techniques, across many platforms, which would achieve the Aharonov–Bohm phase and time-dilation effects predicted here.

The insight that a Dirac self-accelerating wavepacket mimics all properties of a force acting on a charged particle calls for another fundamental question, which we leave open for future work: does a self-accelerating single-electron wavepacket emit radiation? On the one hand, one would naively expect an accelerating particle to radiate; but on the other hand, there is no force acting on the particle, meaning that its overall energy is constant. This and many other questions arise from accelerating particles in free space, because they challenge our closely held intuition about relativistic dynamics.

Received 14 May 2014; accepted 14 November 2014;
published online 5 January 2015

References

- Aharonov, Y. & Bohm, D. Significance of electromagnetic potentials in the quantum theory. *Phys. Rev.* **115**, 485–491 (1959).
- Berry, M. V. Quantal phase factors accompanying adiabatic changes. *Proc. R. Soc. Lond. A* **392**, 45–57 (1984).
- Fang, K., Yu, Z. & Fan, S. Photonic Aharonov–Bohm effect based on dynamic modulation. *Phys. Rev. Lett.* **108**, 153901 (2012).
- Fang, K., Yu, Z. & Fan, S. Experimental demonstration of a photonic Aharonov–Bohm effect at radio frequencies. *Phys. Rev. B* **87**, 060301 (2013).
- Li, E., Eggleton, B. J., Fang, K. & Fan, S. Photonic Aharonov–Bohm effect in photon–phonon interactions. *Nature Commun.* **5**, 3225 (2014).
- Anandan, J. & Aharonov, Y. Geometric quantum phase and angles. *Phys. Rev. D* **38**, 1863 (1988).
- Hohensee, M. A., Estey, B., Hamilton, P., Zeilinger, A. & Müller, H. Force-free gravitational redshift: Proposed gravitational Aharonov–Bohm experiment. *Phys. Rev. Lett.* **108**, 230404 (2012).
- Kane, C. L. & Mele, E. J. Quantum spin Hall effect in graphene. *Phys. Rev. Lett.* **95**, 226801 (2005).

9. Bernevig, B. A., Hughes, T. L. & Zhang, S. C. Quantum spin Hall effect and topological phase transition in HgTe quantum wells. *Science* **314**, 1757–1761 (2006).
10. Wang, Y. H., Steinberg, H., Jarillo-Herrero, P. & Gedik, N. Observation of Floquet–Bloch states on the surface of a topological insulator. *Science* **342**, 453–457 (2013).
11. Rechtsman, M. C. *et al.* Photonic Floquet topological insulators. *Nature* **496**, 196–200 (2013).
12. Rechtsman, M. C. *et al.* Strain-induced pseudomagnetic field and photonic Landau levels in dielectric structures. *Nature Photon.* **7**, 153–158 (2013).
13. Hafezi, M., Mittal, S., Fan, J., Migdall, A. & Taylor, J. M. Imaging topological edge states in silicon photonics. *Nature Photon.* **7**, 1001–1005 (2013).
14. Struck, J. *et al.* Quantum simulation of frustrated classical magnetism in triangular optical lattices. *Science* **333**, 996–999 (2011).
15. Aidelsburger, M. *et al.* Experimental realization of strong effective magnetic fields in an optical lattice. *Phys. Rev. Lett.* **107**, 255301 (2011).
16. Jimenez-Garcia, K. *et al.* Peierls substitution in an engineered lattice potential. *Phys. Rev. Lett.* **108**, 225303 (2012).
17. Struck, J. *et al.* Tunable gauge potential for neutral and spinless particles in driven optical lattices. *Phys. Rev. Lett.* **108**, 225304 (2012).
18. Dirac, P. A. M. The quantum theory of the electron. *Proc. R. Soc. Lond. A* **117**, 610–624 (1928).
19. Geim, A. & Novoselov, K. The rise of graphene. *Nature Mater.* **6**, 183–191 (2007).
20. Peleg, O. *et al.* Conical diffraction and gap solitons in honeycomb photonic lattices. *Phys. Rev. Lett.* **98**, 103901 (2007).
21. Salger, T., Grossert, C., Kling, S. & Weitz, M. Klein tunneling of a quasirelativistic Bose–Einstein condensate in an optical lattice. *Phys. Rev. Lett.* **107**, 240401 (2011).
22. Windpassinger, P. & Sengstock, K. Engineering novel optical lattices. *Rep. Prog. Phys.* **76**, 086401 (2013).
23. Polini, M., Guinea, F., Lewenstein, M., Manoharan, H. C. & Pellegrini, V. Artificial honeycomb lattices for electrons, atoms and photons. *Nature Nanotech.* **8**, 625–633 (2013).
24. Jacqmin, T. *et al.* Direct observation of Dirac cones and a flatband in a honeycomb lattice for polaritons. *Phys. Rev. Lett.* **112**, 116402 (2014).
25. Jacob, Z., Alekseyev, L. V. & Narimanov, E. Optical hyperlens: Far-field imaging beyond the diffraction limit. *Opt. Express* **14**, 8247–8256 (2006).
26. Salandrino, A. & Engheta, N. Far-field subdiffraction optical microscopy using metamaterial crystals: Theory and simulations. *Phys. Rev. B* **74**, 075103 (2006).
27. Katsnelson, M. I., Novoselov, K. S. & Geim, A. K. Chiral tunneling and the Klein paradox in graphene. *Nature Phys.* **2**, 620–625 (2006).
28. McCann, E. *et al.* Weak-localization magnetoresistance and valley symmetry in graphene. *Phys. Rev. Lett.* **97**, 146805 (2006).
29. Atala, M. *et al.* Direct measurement of the Zak phase in topological Bloch bands. *Nature Phys.* **9**, 795–800 (2013).
30. Segev, M., Solomon, R. & Yariv, A. Manifestation of Berry's phase in image-bearing optical beams. *Phys. Rev. Lett.* **69**, 590 (1992).
31. Siviloglou, G. A., Broky, J., Dogariu, A. & Christodoulides, D. N. Observation of accelerating Airy beams. *Phys. Rev. Lett.* **99**, 213901 (2007).
32. Baumgartl, J., Mazilu, M. & Dholakia, K. Optically mediated particle clearing using Airy wavepackets. *Nature Photon.* **2**, 675–678 (2008).
33. Polynkin, P., Kolesik, M., Moloney, J. V., Siviloglou, G. A. & Christodoulides, D. N. Curved plasma channel generation using ultraintense Airy beams. *Science* **324**, 229–232 (2009).
34. Chong, A., Renninger, W. H., Christodoulides, D. N. & Wise, F. W. Airy–Bessel wave packets as versatile linear light bullets. *Nature Photon.* **4**, 103–106 (2010).
35. Kaminer, I., Segev, M. & Christodoulides, D. N. Self-accelerating self-trapped optical beams. *Phys. Rev. Lett.* **106**, 213903 (2011).
36. Lotti, A. *et al.* Stationary nonlinear Airy beams. *Phys. Rev. A* **84**, 021807 (2011).
37. Dolev, I., Kaminer, I., Shapira, A., Segev, M. & Arie, A. Experimental observation of self-accelerating beams in quadratic nonlinear media. *Phys. Rev. Lett.* **108**, 113903 (2012).
38. Kaminer, I., Bekenstein, R., Nemirovsky, J. & Segev, M. Nondiffracting accelerating wave packets of Maxwell's equations. *Phys. Rev. Lett.* **108**, 163901 (2012).
39. Bekenstein, R., Nemirovsky, J., Kaminer, I. & Segev, M. Shape-preserving accelerating electromagnetic wave packets in curved space. *Phys. Rev. X* **4**, 011038 (2014).
40. Voloch-Bloch, N., Lereah, Y., Lilach, Y., Gover, A. & Arie, A. Generation of electron Airy beams. *Nature* **494**, 331–335 (2013).
41. Berry, M. V. & Balazs, N. L. Nonspreading wave packets. *Am. J. Phys.* **47**, 264–267 (1979).
42. Einstein, A. On the electrodynamics of moving bodies. *Ann. Phys. Lpz.* **17**, 891–921 (1905).
43. Batelaan, H. & Tonomura, A. The Aharonov–Bohm effects: Variations on a subtle theme. *Phys. Today* **62**, 38–43 (September, 2009).
44. Cohen-Tannoudji, C., Diu, B. & Laloe, L. *Quantum Mechanics* Vol. 1 (Wiley-VCH, 1991).
45. Sepkhanov, R. A., Bazaliy, Ya. B. & Beenakker, C. W. J. Extremal transmission at the Dirac point of a photonic band structure. *Phys. Rev. A* **75**, 6 (2007).
46. Zewail, A. H. Four-dimensional electron microscopy. *Science* **328**, 187–193 (2010).
47. Berry, M. V., Jeffrey, M. R. & Lunney, J. G. Conical diffraction: Observations and theory. *Proc. R. Soc. Lond. A* **462**, 1629–1642 (2006).

Acknowledgements

We thank R. L. Jaffe for valuable discussions that considerably contributed to our work. This research was funded by the ICore Excellence Center 'Circle of Light', by the Binational USA–Israel Science Foundation BSE, and by a Marie Curie Grant no 328853–MC–BSiCS.

Author contributions

All authors contributed to all aspects of this work.

Additional information

Supplementary information is available in the [online version of the paper](#). Reprints and permissions information is available online at www.nature.com/reprints. Correspondence and requests for materials should be addressed to I.K.

Competing financial interests

The authors declare no competing financial interests.